Transition to turbulent heat transfer in heated vertical channel - Experimental analysis

Christophe Daverat, Yiqin Li, Hervé Pabiou, Christophe Ménézo, Shihe Xin

▶ To cite this version:

HAL Id: hal-01393834
https://hal.science/hal-01393834v2

Submitted on 13 Feb 2018

Transition to turbulent heat transfer in heated vertical channel - Experimental analysis

C. Daverat[a], Y. Li[a,c], H. Pabiou[a,*], C. Ménézo[a,b], S. Xin[a]

[a] Univ Lyon, CNRS, INSA-Lyon, Universit Claude Bernard Lyon 1, CETHIL UMR5008, F-69621, Villeurbanne, France
[b] Chaire INSA/EDF, Habitats et Innovations Energétiques, Lyon, France
[c] Agence de l'Environnement et de la Maîtrise de l'Énergie 20, avenue du Grésillé- BP 90406 49004 Angers Cedex 01 France

Abstract

This experimental study deals with natural convection flow in a water channel with a symmetrical isoflux wall heating. Wall temperature, velocity, bulk temperature and fluctuating quantities are measured for a modified Rayleigh number $Ra^* = 6.7 \times 10^7$. The analysis of the mean values shows a change of behaviour at the two-third of the height of the channel. This change turns out to be a transition from a laminar heat transfer in the bottom part of the channel to a turbulent one in the upper part. Due to isoflux wall boundary conditions, shear layers develop and thicken in each half-channel. It is shown that the meeting of these layers at the centre of the channel triggers the transition from a laminar heat transfer to a turbulent one. This experimental study is followed by a scaling analysis [1].

Keywords: Natural convection, turbulent heat transfer, vertical open channel, shear layer
PACS: 47.55.pb, 44.25.+f, 44.15.+a, 47.27.te

1. Introduction

Natural convection in open-ended vertical channels has been investigated for decades thanks to its broad application fields (electronic, solar systems,

---

[*]Corresponding author
Email address: herve.pabiou@insa-lyon.fr (H. Pabiou)

buildings,...). With isoflux wall boundary conditions, the flow can be characterized by the modified Rayleigh number: $Ra^* = \frac{g\beta q_\mathrm{w} b^5}{\lambda \nu \kappa H}$; where g is the gravitational acceleration, q_w the wall heat flux, b and H the width and height of the channel, and β, ν, λ, κ the isobaric thermal expansion coefficient, kinematic viscosity, thermal conductivity and thermal diffusivity of the fluid, respectively. The Rayleigh number compares buoyant effects that tend to lift the fluid upward with viscous dissipation and thermal diffusion that tend to counteract the buoyant effect. This definition is the most commonly used but there is no evidence showing that it is the only parameter that characterizes the flow behaviour. The natural convection flow at low Rayleigh number ($Ra^* < 10^5$) has been fully investigated for years [2, 3, 4, 5], and analytical solutions have been developed [6]. However, many applications such as photovoltaic double-skin façades [7], are characterized by higher Rayleigh number ($Ra^* \sim 10^{10}$) where natural convection flow undergoes a transition to turbulence. Flows at these ranges of high Rayleigh numbers were much less investigated.

Miyamoto *et al.*[8] carried out one of the first experimental studies on turbulent natural convection flow in a 5 m high vertical air channel. One wall is heated with a constant heat flux, the other wall being adiabatic. They performed wall temperature measurements by using thermocouples and velocity measurements in the channel with a Laser Doppler Velocimetry (LDV) system for several aspect ratios ($H/b = 100, 50$ and 25). The wall temperature profile exhibits a maximum value located between 1 and 2 m from the channel inlet for three Rayleigh numbers Ra^* ranging from 7×10^3 to 2×10^7. They attributed this maximum to a transition from laminar to turbulent flow. Vertical velocity and temperature profiles are shown at three vertical positions in the channel for the three aspect ratios. The increase in the vertical velocity as the fluid rises along the heated wall is clearly seen for the experiment with the largest aspect ratio whereas the behaviour is not clear for the lower ones. Indeed, for the lowest aspect ratio, the velocity peak does not increase until the end of the channel, a decrease is seen in the upper part. This decrease comes with an increase in the temperature of the fluid in the whole section. Despite the difference in the experimental setups, this behaviour could be similar to the one described in this study.

Later, Webb and Hill [9] analysed heat transfer in a configuration close to Miyamoto's but adiabatic extensions have been added at the entry and the exit of the channel. The channel height is 15 cm. The 7.62 cm high heated

zone is vertically centred on one wall. In the range $10^3 \leqslant Ra^* \leqslant 4 \times 10^7$, no transition is observed. For the most efficient heat transfer, the Nusselt number based on the channel width is found to be proportional to the modified Rayleigh number raised to the power of 1/5 which means that heat transfer is independent of the channel width as in the case of the vertical flat plate ([10]).

More recently, Habib *et al.* [11, 12, 13] performed LDV and Particles Images Velocimetry (PIV) measurements on a 12.5 cm high channel with isothermal heating (symmetrical and asymmetrical heating). They presented several results on turbulent quantities with numerical validations. The comparisons focused on the influence of the width and no much information were given on the evolution along the channel.

Fossa *et al.*[14] as well as Brinkworth and Sandberg[7] have carried out experimental studies in vertical channels with isoflux heating on one wall, the other one being adiabatic. As Miyamoto did, they observed a maximum on the heated wall temperature profile. This maximum appears around the three-quarters of the height of the channel with a sharp decrease at the outlet. Sanvicente *et al.* [15] published a study completing the one of Fossa *et al.*[14] by using the same configuration with a 1.5 m high channel. A wall temperature decrease is also shown in the upper third of the channel height. They associated this maximum to a change in flow regime which is probably combined with the effect of radiative heat losses to the surrounding. This change is visualized by Particles Image Velocimetry (PIV) measurements that show an increase in the velocity fluctuations at the channel outlet.

Concerning numerical studies, Fedorov and Viskanta[16] were among the first to carry out simulations in this configuration in the same range of Rayleigh numbers. They analysed cases of both isoflux and isothermal heating on one wall, the other one being adiabatic. They used a k-ε low Reynolds number model and they addressed the problem of boundary conditions at the channel inlet. The influence of the inlet turbulent intensity was investigated and results were compared with Miyamoto's in the isoflux case. Finally, for an aspect ratio of $H/b = 50$ and $Ra^* = 7 \times 10^5$, they showed that without considering inlet turbulence, the transition to turbulence occurs at $x = 3.8$ m from the channel inlet whereas it occurs at $x = 1.8$ m in the experimental study. The transition moves upstream as the Rayleigh number or the inlet turbulence intensity increases.

Cheng and Müller[17] studied turbulent natural convection numerically and experimentally. One wall was isothermally heated and the other was

insulated. The simulations were performed with a k-ε turbulence model and took radiative heat transfer between walls into account, but the inlet conditions were not described in detail. Comparisons with a 8 m high experimental air channel showed a good agreement but the study was mainly focused on the thermal heat transfer and the turbulent characteristics of the flow were not investigated.

Yilmaz and Fraser [18] presented a numerical and experimental study on a 3 m high vertical channel with isothermal heating: one wall heated and the other adiabatic. They tested 3 different k-ε models and neglected radiative heat transfer. In the numerical study, they used the experimental turbulent intensity at the inlet as a boundary condition. However, the comparison with LDV measurements showed that numerical turbulent kinetic energy profiles did not match the experimental ones.

To investigate the impact of boundary conditions on numerical simulation of natural convection flow in a vertical open channel, benchmark solutions based on the configuration of Webb and Hill [9] were given by Desrayaud et $al.$ [19]. It appears that the thermal field is weakly dependent on the inlet and and outlet conditions which is not the case for fluid flow quantities (mass flow rate and bulk temperature).

Most of the studies on natural convection in an open-ended channel are focused on asymmetrical heating. Studies on symmetrical configurations are limited to laminar flows ([20], [21]). To investigate this configuration, an experimental apparatus has been set up in order to study turbulent natural convection in a vertical channel with symmetrical isoflux heating conditions. The set-up has already been presented by Daverat et $al.$[22]. The water is chosen as the working fluid to avoid radiative heat transfer between heated walls and their surroundings. A measuring system coupling LDV and a micro-thermocouple has been developed to characterize the interaction between thermal and dynamical behaviours. From the temperature and velocity measurements at the inlet and outlet of the channel, Daverat et $al.$[22] showed a change in the flow behaviour for a modified Rayleigh number $Ra^* \simeq 10^7$. The change was attributed to the development of a strong shear that leads to an increase in the velocity fluctuations. For Rayleigh number higher than 10^7, the fluid mixing is strong enough to reduce the global shear in the channel. The present study focuses on the evolution of the flow along the channel for $Ra^* = 6.7 \times 10^7$ and arguments are brought to complete the first analysis of Daverat et $al.$ [22].

The main features of the experimental apparatus and the characteristics

4

of its metrology are firstly presented. Then, the main flow features based on mean velocity and temperature profiles are shown and heat transfer is analysed in different parts of the channel. Finally, the behaviour of the flow is analysed and the role of shear is highlighted.

Nomenclature

b	Channel width (m)
g	Acceleration of gravity (m s^{-2})
H	Channel height (m)
l	Channel depth (m)
Nu_x	Local Nusselt number, Eq.2
Pr	Prandtl number
q_w	Wall heat flux (W m^{-2})
Ra^*	Modified Rayleigh number, $Ra^* = \frac{g\beta q_\mathrm{w} b^5}{\lambda \nu \kappa H}$
Ra_x	Local Rayleigh number, Eq.1
Re	Reynolds number
$T(x,y)$	Mean temperature (K)
$T_c(x)$	Mean temperature at the channel centre (K)
T_ref	Reference temperature for the Boussinesq approximation (K)
T_inlet	Inlet temperature (K)
$T_{lw}(x)$	Mean temperature of the left wall (K)
U, V, W	Mean velocity component in the directions x, y, z, respectively (m s^{-1})
u', v', w'	Instantaneous velocity fluctuations in the directions x, y, z, respectively (m s^{-1})
$U_\mathrm{max}, U_\mathrm{min}$	Maximum and minimum of the mean vertical velocity profile, respectively (m s^{-1})
x	Distance from the inlet in the ascendant direction (m)
y	Distance from the left wall (m)
y_{uv}	Location of the maximum Reynolds stress at x (m)
y_{SL}	Right boundary location of the shear layer at x, Eq.6, (m)
z	Distance from the front lateral wall (m)

β	Isobaric thermal expansion of water (K^{-1})
$\Gamma = \frac{H}{b}$	Aspect ratio
$\Delta U = U_{\mathrm{max}} - U_{\mathrm{min}}$	Mean vertical velocity difference at x $(\mathrm{m\ s}^{-1})$
δ_ν	Viscous boundary layer thickness, Eq.5, (m)
δ_T	Thermal boundary layer thickness, Eq.3, (m)
$\delta_{T,0}$	Thermal boundary sublayer thickness, Eq.4, (m)
θ'	Instantaneous temperature fluctuations (K)
κ	Thermal diffusivity of water $(\mathrm{m}^2\ \mathrm{s}^{-1})$
λ	Thermal conductivity of water $(\mathrm{W\ m}^{-1}\ \mathrm{K}^{-1})$
ν	Cinematic viscosity of water $(\mathrm{m}^2\ \mathrm{s}^{-1})$
$\sigma_u, \sigma_v, \sigma_w$	Root mean square of the velocity fluctuations u', v', w', respectively $(\mathrm{m\ s}^{-1})$
σ_θ	Root mean square of the temperature fluctuations(K)
$<>$	Time average operator

2. Experimental apparatus

2.1. Experimental set-up

The experimental apparatus (Fig. 1) has been already described and characterized in detail in Daverat *et al.*[22] and main features are summarized below. A 65 cm high (x direction), $b = 5.9$ cm wide (y direction) and $l = 23.5$ cm deep (z direction) vertical channel is located inside a 1.5 m high, 60 cm wide and 23.5 cm deep glass tank filled with water. The vertical channel is open at its top and bottom (x direction) and is delimited by two waterproof boxes in the y direction and by the glass tank in the z direction. Each waterproof box is composed of a polycarbonate frame, a polycarbonate cover and a 1.5 mm thick stainless steel plate which is one of the heated walls of the channel. A natural convection flow develops inside the channel and two back flows go down behind the boxes.

Both channel main walls (stainless steel plates) are heated by 12 independent electrical heaters which apply an isoflux boundary condition as shown on Fig. 1b. The heated surface is $H = 61.1$ cm high and 20 cm wide in the middle of each wall. To reach a modified Rayleigh number $Ra^* = 6.7 \times 10^7$,

a heat flux $q_w = 1150 \text{W.m}^{-2}$ is applied on the two walls, all fluid properties being taken at a reference temperature $T_{\text{ref}} = 35.6°C$ which corresponds to the average of the minimum and maximum temperatures in the channel. In order to limit the heat conduction in x direction between two heated areas, 1 mm deep grooves are engraved, in the inner face of the plate, parallel to the z direction. The water tank is covered by 5 cm thick insulating material with a thermal conductivity of 0.033 $\text{W.m}^{-1}.\text{K}^{-1}$. The water temperature outside the channel is regulated with an external system composed of a pump, a thermo-regulated bath and a heat exchanger. Hot water is pumped out close to the cell walls (far from the channel) and it is discharged at a low velocity behind the waterproof boxes (Fig. 1b). The bench is placed in a room in which the temperature is controlled within $\pm 2°C$.

Heat flux sensors are stuck on the electrical heaters to measure the mean heat flux injected in the channel by each heater. Temperatures are measured with 130 μm diameter K-type thermocouples. The temperature of the walls is measured at the centre of each heater by 2×12 thermocouples located in 1 mm deep grooves. Temperature is also measured at the channel inlet and outlet, at the bottom and top of the tank, at the suction and discharge points of the water cooling system and in the waterproof boxes as shown on Figure 1. All the temperature measurements are made in the central plane xOy of the channel located at $z/l = 0.5$.

Velocity and temperature are measured in the flow. A micro-thermocouple (25 μm K-type) and a two-component LDV system are mounted on a two directional (x, y) moving system. Therefore, temperature and velocity components in the x and y directions are measured in the channel central plane. The micro-thermocouple is located 1 mm above the LDV measurement volume to avoid interaction with the laser beams. The seeding particles are 5 μm polyamide spheres with a density of 1.03 kg.m^{-3}. The sampling rate for velocity measurement is in the range of $[3 - 10]$ Hz and the measurement duration is one hour. The sampling rate for bulk temperature measurements is 9 Hz.

2.2. Characterization of the bench

The heat losses by the lateral walls were estimated to be around 1 % of the injected heat flux. Therefore, an adiabatic boundary condition is assumed for the channel lateral walls.

The fluctuations of the velocity at the channel inlet $(x/H = 0.04)$ are high. Indeed, the turbulent intensity is around 35 % and the minimum
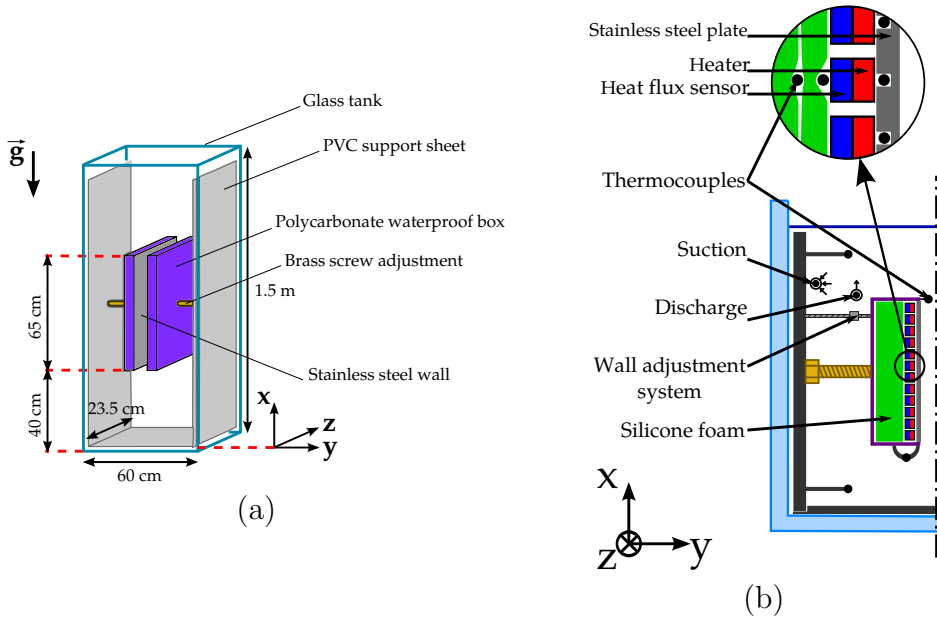
7

Figure 1: (a) Scheme of the experimental apparatus. (b) Detailed view of the left half-apparatus. Symbols (●) are the positions of the thermocouples. The movable micro-thermocouple is not shown.

duration needed to ensure the convergence of the mean velocity within 1% is five hours [22]. As it may be difficult to maintain constant ambient conditions in the room during several weeks, the measurement duration is chosen as a compromise between the duration of the measurements and the accuracy on the averaged velocities. The choice of one hour allows to perform the measurement of a complete profile ($\sim$ 22 measuring points) in one day with an uncertainty limited within ± 4 %.

The most tricky point of the velocity and temperature measurements in the channel is the determination of the distance between the measuring point and the wall. In order to perform measurements very close to the left wall of the channel, the LDV laser probe is tilted at an angle of 4° with respect to the normal to the front wall of the glass tank and the refractive effects are corrected by adding a prismatic glass cell filled with water in front of the main glass tank. In this configuration, the distance of the measuring point to the wall is not known precisely. Therefore a localisation method is developed in order to estimate the distance between the measuring point and the left wall. This method is based on the relationship between the wall heat flux

(measured by the heat flux sensors) and the temperature profile close to the wall (measured by the micro-thermocouple) and the wall temperature [22]. The uncertainty introduced by this method on channel width is ± 1 mm. Due to a defect in the parallelism of the walls, the width is known within ± 3 mm, which is the main source of uncertainty on Ra^* value. Moreover, thermocouples and heat flux sensors were calibrated in the laboratory and the uncertainty on temperature and heat flux measurements are $\pm 0.1°$C and $< 1\%$ of the heat flux injected in the channel, respectively.

3. Results and discussion

The results presented in this study correspond to a modified Rayleigh number $Ra^* = 6.7 \times 10^7 \pm 25\%$, a Prandtl number at the inlet temperature $Pr = 4.9$, a Reynolds number based on the bulk velocity and the width of the channel $Re = 570 \pm 10\%$ and an aspect ratio $\Gamma = \frac{H}{b} = 10.4 \pm 5\%$. U, V, W and T denote the mean velocity components along x, y, z and the mean temperature, respectively. u', v', w' and θ' denote the corresponding instantaneous fluctuations whereas σ_u, σ_v, σ_w and σ_θ are the RMS values.

3.1. Mean flow behaviour

Figure 2a shows the mean vertical velocity profiles over the half-width of the channel for 11 vertical positions. At the channel inlet ($x/H = 0.12$), the profile is flat. In the bottom part of the channel ($x/H \leqslant 0.71$), velocity increases along the x-axis close to the heated wall ($y/b = 0$) under buoyant effect and decreases at the centre of the channel ($y/b = 0.5$) due to mass conservation. We define $U_{\max}(x)$ and $U_{\min}(x)$ as the maximum and minimum values of each mean velocity profile measured at the vertical position x. $U_{\min}$ is the average value of 3 measurements performed around the centre of the channel ($y/b = 0.5$) to limit uncertainty. The velocity gradient characterized by the velocity difference $\Delta U(x) = U_{\max}(x) - U_{\min}(x)$ creates a shear layer between the maximal peak close to the wall and the centre of the channel. Figure 2b shows that $\Delta U(x)$ exhibits a maximum value at $x/H = 0.71$. Above this position, the mean flow behaves differently: velocity decreases close to the heated wall and increases at the centre of the channel.

A similar change is observed on mean temperature. Figure 3a shows the mean temperature profiles for 11 vertical positions. Figures 3b-c show the mean temperature of the left wall $T_{lw}(x) = T(x, y = 0)$ and the temperature at the channel centre $T_c(x) = T(x, y = 0.5b)$. Temperature at the centre is
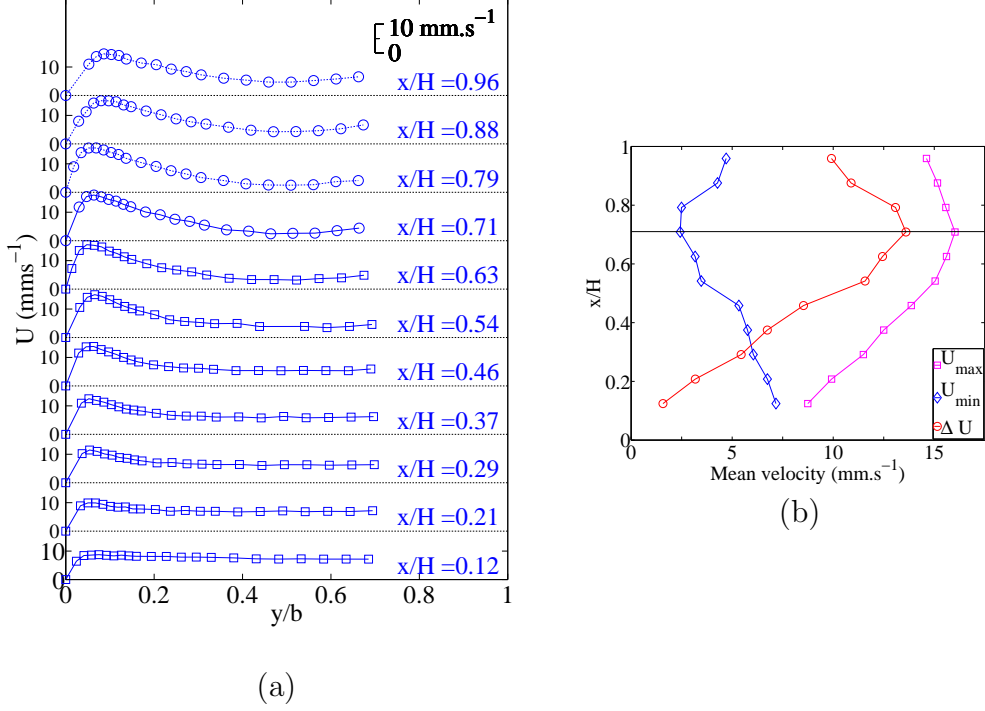
Figure 2: (a) Mean vertical velocity profiles for 11 vertical positions. Profiles are shifted for clarity. Markers ($\square$) and (o) indicate the parts of the channel where ΔU increases and decreases, respectively; (b) Maximum mean velocity, minimum mean velocity at the centre and velocity difference for 11 vertical positions along the channel. The horizontal line is $x/H = 0.71$.

the average of 3 measurements performed around $y/b = 0.5$. On Figure 3b the small bump on the wall temperature profile at $x/H = 0.63$ is attributed to an uncertainty in the position of the corresponding thermocouple. Figure 3b shows that wall temperature increases up to $x/H = 0.46$; remains almost constant between $x/H = 0.54$ and $x/H = 0.79$; then decreases. In the centre of the channel, temperature remains constant below $x/H = 0.71$, and exhibits a jump at $x/H = 0.71$. This behaviour can also be shown in non dimensional variables. Equations 1 and 2 are the definitions of a local
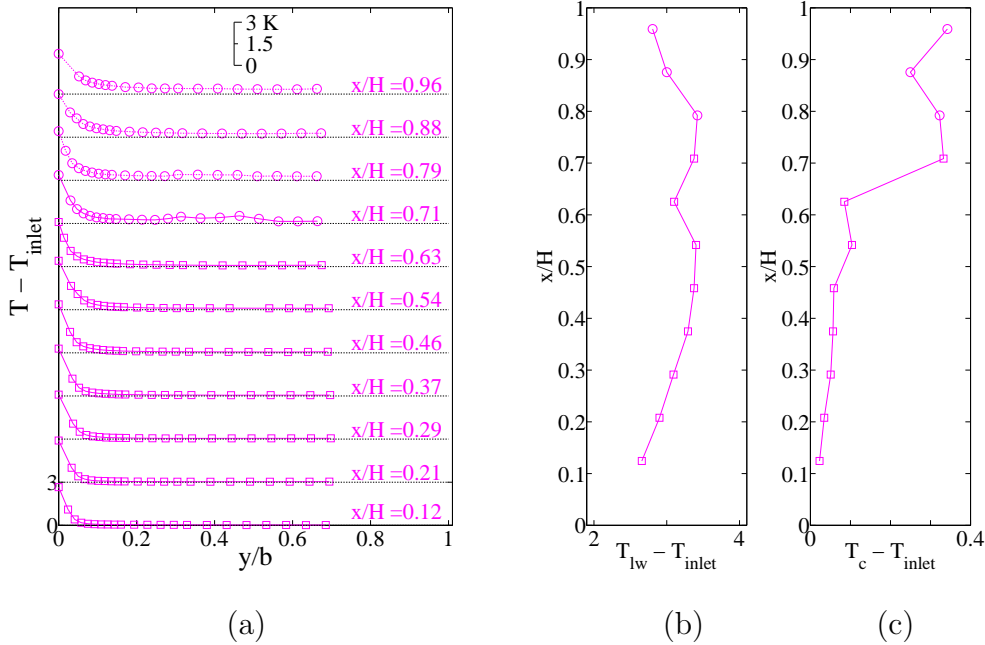
10

Figure 3: (a) Mean temperature profiles for 11 vertical positions. Profiles are shifted for clarity. Markers ($\square$) and (o) indicate the parts of the channel where ΔU increases and decreases, respectively; Temperature of the left wall (b) and temperature at the centre of the channel (c) shifted by the inlet temperature for 11 vertical positions along the channel. The wall temperature at $x/H = 0.63$ is undervalued because the thermocouple is not well embedded in the plate.

Rayleigh number and a local Nusselt number, respectively.

$$Ra_x = \frac{g\beta q_{\mathrm{w}} x^4}{\lambda \nu \kappa} \tag{1}$$

$$Nu_x = \frac{q_{\mathrm{w}} x}{\lambda (T_{lw} - T_{\mathrm{inlet}})} \tag{2}$$

Figure 4 shows the Nusselt number versus the Rayleigh number along the channel. The plot Nusselt number is compensated by $Ra_x^{1/5}$ to enlarge the vertical axis. A constant value corresponds to the power law $Nu_x \propto Ra_x^{1/5}$ that holds for a laminar vertical flat plate ([10]). This choice is explained by the scaling analysis [1]. The change of behaviour is shown by the slope increase in Figure 4.

This change of behaviour characterized by a maximum on $\Delta U(x)$, a sudden increase in $T_c(x)$ and a change of slope of the curve $Nu_x = f(Ra_x)$ is a
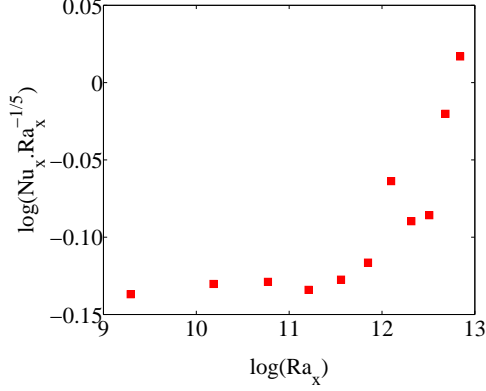
Figure 4: Nusselt number versus Rayleigh number along the channel.

key point that is analysed in this study. In what follows, we denote *bottom part* and *upper part* of the channel the areas located below and above $x/H = 0.71$, respectively.

Mean velocity and temperature values at $Ra^* = 6.7 \times 10^7$ are given in appendix (Table A.1). They can be used as reference data for numerical simulations for this configuration.

3.2. Laminar heat transfer in the bottom part

Thermal boundary layer (TBL) thickness δ_T is usually defined by:

$$
\begin{aligned}
T(x, y_T) - T_{\text{inlet}} &= a(T_{lw} - T_{\text{inlet}}) \\
\delta_T &= \min\left(y_T, \frac{b}{2}\right)
\end{aligned}
\tag{3}
$$

where a is a coefficient that is usually equal to 1%. However, due to the uncertainty on the temperature, such a low coefficient would lead to undetectable temperature $T(x, \delta_T) - T_{\text{inlet}}$. Therefore, in this study, a value of $a = 0.075$ is chosen. Thus, for a wall heating around 1°C, the temperature at the edges of the TBLs is 0.075°C, which remains detectable. However, this definition is not linked to the wall temperature gradient which is a key parameter for the wall heat transfer. Therefore, we also define a thermal boundary sublayer (TBsL) thickness $\delta_{T,0}$, as the ratio of the wall temperature to the corresponding normal temperature gradient:

$$
\delta_{T,0} = \frac{\lambda(T_{lw} - T_{\text{inlet}})}{q_w}
\tag{4}
$$

12

The TBsL is nested inside the TBL and it concentrates most of the temperature gradient. Concerning the viscous boundary layer (VBL), we define its thickness $\delta_\nu(x)$ as the displacement thickness,

$$U(x, y_{\max}) = \max_{0 \le y \le b/2} U(x,y) = U_{\max}(x)$$

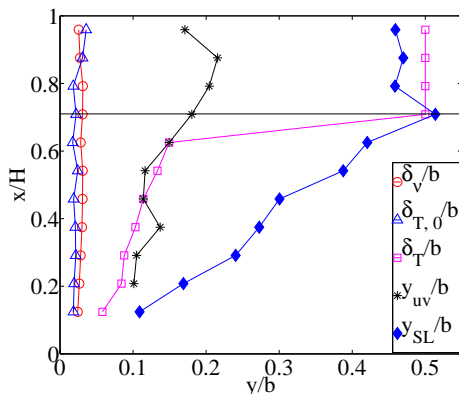$$\delta_\nu = \int_0^{y_{\max}} \left(1 - \frac{U}{U_{\max}}\right) dy. \tag{5}$$

Figure 5: Typical horizontal lengths : thermal boundary layer thickness (δ_T, Eq. 3), thermal boundary sublayer thickness ($\delta_{T,0}$, Eq. 4), displacement dynamic boundary layer thickness (δ_ν, Eq. 5), location of the maximum Reynolds stress (y_{uv}) and right boundary location of the shear layer (y_{SL}, Eq.6). The horizontal line is $x/H = 0.71$.

$\delta_{T,0}(x)$ and $\delta_\nu(x)$ are shown on Figure 5 and these two thickness appear to be of the same order of magnitude. Indeed, as the driving force of the flow acts mainly inside the TBsL, the velocity gradient is concentrated inside this layer and therefore, the maximum velocity is located near the edge of the TBsL.

Concerning the TBL thickness δ_T shown on Figure 5, it experiences a jump at $x/H = 0.71$ which is a signature of the transition from a laminar heat transfer in the bottom part to a turbulent one in the upper part.

3.3. Turbulent heat transport in the upper part

Turbulent heat transfer in the upper part means that heat is directly transported by hot particles that travel from the laminar TBsL to the center of the channel. In order to characterize this kind of heat transfer, the

horizontal turbulent heat flux is estimated from velocity and temperature measurements.

However, velocity and temperature measurements are neither performed exactly at the same location nor with the same acquisition rate. Therefore the cross-correlation between horizontal velocity and temperature fluctuations $<v'\theta'>$, which characterizes the mean horizontal turbulent heat flux, can not be calculated exactly but can be estimated as proposed by Shang et al. [23, 24]. Temperature measurements, which have the higher rate of data acquisition, are resampled to match the rate of the velocity measurements. This resampling does not introduce an error on the mean temperature value but it induces an uncertainty of around 5-10 % on the temperature standard deviation. Moreover, one hour measurement is not sufficient to reach the convergence of the mean value, which increases the uncertainty. This estimate $<v'\theta'>_{\text{estim}}$ takes into account the flow structures with a size greater than 1 mm and with a correlation time longer than 0.3 s as it corresponds to the distance between the velocity and temperature measurement locations and to the mean sampling rate of the velocity, respectively. As $<v'\theta'>$ is not exactly quantified, the following analysis is only qualitative.

Figure 6 shows a map of the estimation of the horizontal turbulent heat flux in which values are linearly interpolated from the discrete set of data. We observe two different behaviours below and above $x/H = 0.71$. In the bottom part, the horizontal turbulent heat-flux is low which is consistent with
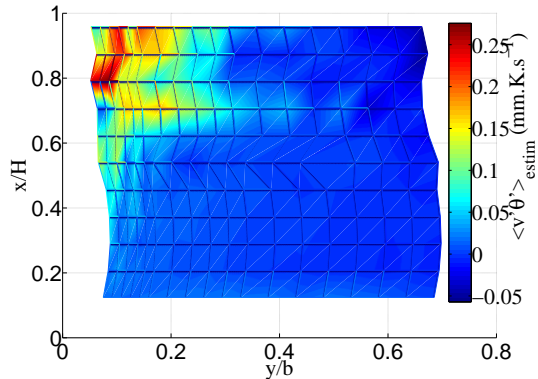

Figure 6: Estimate of the cross-correlation between horizontal velocity and temperature fluctuations. The colormap is built from a linear interpolation of the discrete set of data and the broken lines are the edges of the mesh.

14

a laminar heat transfer in the TBL. In the upper part, horizontal turbulent heat flux increases close to the wall meaning that hot structures travel from the TBsL toward the centre of the channel. The increase in the turbulent heat flux in the upper part is responsible for the increase in temperature in the centre of the channel as shown on Figure 3b.

3.4. Scenario of transition

To understand the mechanism that leads to this transition, a focus has to be done on the shear layers that develop in the channel. Figure 2a shows that the fluid layer located between the velocity peak and the centre of the channel is subjected to a strong shear. Its left boundary is limited by the velocity peak $(y = y_{\max})$ and we choose to define its right boundary y_{SL} as the closest position from the centre where:

$$U(x, y_{SL}) = 1.2 U_{\min} \tag{6}$$

The coefficient 1.2 is chosen to be consistent with the uncertainty. Indeed, with an uncertainty of $\pm 4\%$ on the velocity, the difference $U(x, y_{SL}) - U_{\min}$ is much larger than the noise. The value of $y_{SL}(x)$ is plotted on Fig. 5. Due to momentum diffusion, the shear layers located in the left and right half-channels thicken along the channel until the location of the transition $(x/H = 0.71)$, where they come across each other.

Due to the isoflux boundary condition, the temperature of the fluid, and thus its velocity, increases as it rises along the heated plates. This acceleration can be characterized by the increase in $U_{\max}$ with respect to x in the bottom part . Supposing a two-dimensional flow and according to mass conservation, this increase implies a decrease in the velocity at the centre of the channel, which is characterized by the decrease in $U_{\min}$ (Figure 2b). Therefore two shear layers develop outside the TBLs.

Figures 7 show the RMS fluctuations of the velocity components σ_u, σ_v, of the temperature σ_T and the cross-term of the Reynolds stress $\langle u'v' \rangle$. Maps are obtained from linear interpolation of the discrete set of measurements. Due to the symmetry of the problem, maps are supposed to be symmetrical with respect to $y/b = 0.5$. In the centre of the channel, close to the entry $(x/H \lesssim 0.4, 0.3 \lesssim y/b \lesssim 0.7)$, σ_u and σ_v exhibit a decrease along the x-axis which is related to a relaminarisation of the flow as it enters the channel. Figures 7a, b and d show that σ_u and $\langle u'v' \rangle$ increase along x in the shear layer in the bottom part whereas σ_v increases at a lower rate. The increase
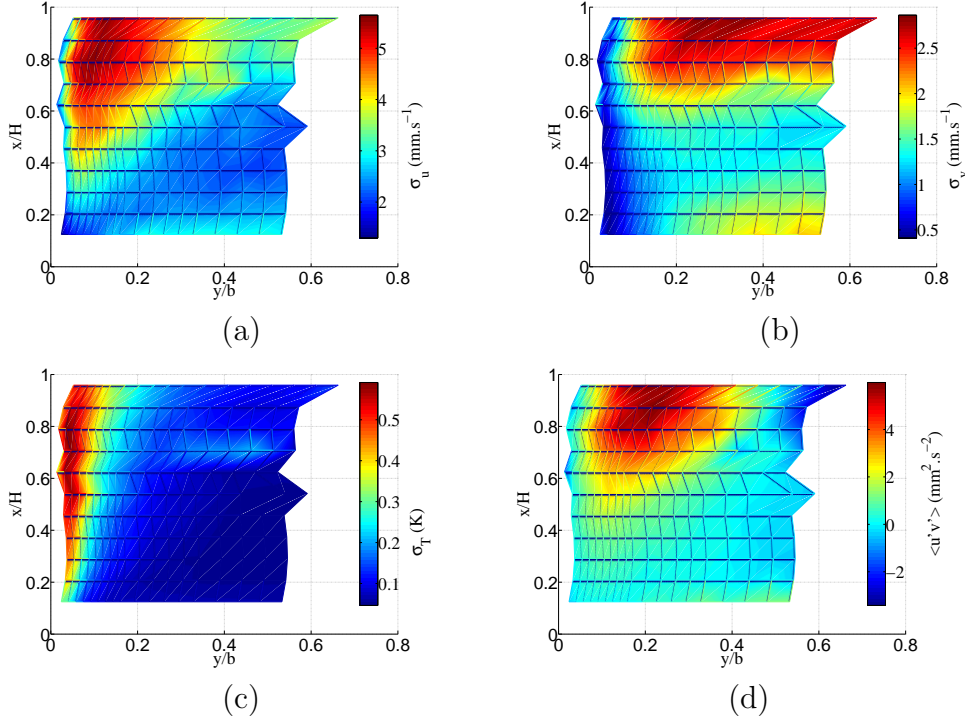
Figure 7: Root mean square of the velocity and temperature fluctuations, and Reynolds stress in the channel. Values are linearly interpolated from the discrete set of data. The broken lines are the edges of the mesh. (a) σ_u (b) σ_v (c) σ_T, (d) $\langle u'v' \rangle$.

in $\langle u'v' \rangle$ indicates an increase in the momentum diffusion due to the velocity fluctuations that thickens the shear layers along the x axis.

At $x/H = 0.71$, the shear layers from the left and right half-channels meet meaning that the momentum diffuses to the centre of the channel, which tends to counteracts the decrease in velocity at the centre. If the decrease in $U_{\min}$ is limited, so is the increase in $U_{\max}$. By continuity, one can suppose that a decrease in $U_{\max}$ (Figure 2b) leads to a decrease in the VBL velocity scale. In the same way, a decrease in the wall temperature (Figure 3b) leads to a decrease in the TBsL temperature scale. Therefore, above the transition, the heat transported in the TBsL decreases. As a consequence, an energy budget inside an horizontal slice of TBsL above the transition shows that an increase in the heat transported from the TBsL to the bulk flow is necessary to balance the heat injected at the wall. According to this scenario, the junction of the shear layers triggers the transition from a laminar regime to

a turbulent heat transfer from the TBsL toward the centre of the channel.

Above $x/H = 0.71$, the turbulent transport of heat results in the heating of the fluid at the centre and the decrease in the wall temperature (Fig. 3b). In the upper part, fluctuations are no longer driven by the shear as the mean shear shear decreases whereas the fluctuations remains almost independent on x (Figures 7a, b anc d). This scenario is confirmed by the scaling analysis in [1].

4. Conclusions

This experimental study deals with transition from a laminar heat transfer to a turbulent one in a vertical channel with symmetrical isoflux conditions and without radiative heat transfer. The transition is found to be triggered by the shear layers that thicken outside the thermal boundary sublayers. To our knowledge, this is the first study that investigates the local process of transition in a vertical channel. As the shear is highly dependent on the geometry, one may expect the aspect ratio to play an essential role in the occurrence of the transition. Moreover, this scenario may hold for the case of a vertical channel heated on one wall which is a classical configuration encountered in various applications such as photovoltaic double-skin façade.

Acknowledgements

Appendix A. Data table : Temperature and velocity

x/H = 0.12 $T_{inlet}=33.9°C$			x/H = 0.21 $T_{inlet}=34.0°C$			x/H = 0.29 $T_{inlet}=33.9°C$			x/H = 0.37 $T_{inlet}=33.9°C$			x/H = 0.46 $T_{inlet}=34.0°C$			x/H = 0.54 $T_{inlet}=34.0°C$		
$\frac{y}{b}$	U	ΔT	$\frac{y}{b}$	U	ΔT	$\frac{y}{b}$	U	ΔT	$\frac{y}{b}$	U	ΔT	$\frac{y}{b}$	U	ΔT	$\frac{y}{b}$	U	ΔT
0.00	0.0	2.7	0.00	0.0	2.9	0.00	0.0	3.1	0.00	0.0	3.3	0.00	0.0	3.4	0.00	0.0	3.4
0.02	6.4	1.1	0.03	8.9	1.0	0.04	10.2	1.1	0.04	10.9	1.2	0.03	11.5	1.5	0.03	10.6	1.7
0.04	8.4	0.4	0.05	9.9	0.4	0.05	11.5	0.5	0.05	12.5	0.6	0.05	13.7	0.7	0.05	14.1	1.1
0.06	8.6	0.2	0.07	9.9	0.2	0.07	11.0	0.3	0.07	11.9	0.3	0.06	13.9	0.5	0.07	15.0	0.6
0.07	8.7	0.1	0.08	9.4	0.1	0.09	10.1	0.2	0.09	11.3	0.2	0.08	12.8	0.3	0.08	14.5	0.4
0.09	8.5	0.1	0.10	8.7	0.1	0.10	9.7	0.1	0.10	10.4	0.2	0.10	12.0	0.2	0.10	13.3	0.3
0.11	8.3	0.1	0.12	8.4	0.1	0.12	8.8	0.1	0.12	9.7	0.2	0.11	11.1	0.2	0.12	12.0	0.3
0.13	8.6	0.1	0.13	8.5	0.1	0.14	8.6	0.1	0.14	8.9	0.1	0.13	10.0	0.2	0.13	10.9	0.2
0.14	8.3	0.1	0.15	7.8	0.1	0.16	8.0	0.1	0.15	8.5	0.1	0.15	9.1	0.1	0.15	10.1	0.2
0.16	8.2	0.0	0.17	7.8	0.1	0.17	7.7	0.1	0.17	8.2	0.1	0.16	8.4	0.1	0.17	9.3	0.2
0.19	8.1	0.0	0.20	7.6	0.0	0.21	7.0	0.1	0.20	7.4	0.1	0.20	7.4	0.1	0.20	8.0	0.2
0.23	8.1	0.0	0.24	7.0	0.0	0.24	7.1	0.1	0.24	6.7	0.1	0.23	6.8	0.1	0.24	6.2	0.1
0.26	7.9	0.0	0.27	7.3	0.0	0.27	6.6	0.0	0.27	6.4	0.1	0.27	6.3	0.1	0.27	5.6	0.1
0.30	7.9	0.0	0.30	7.0	0.0	0.31	6.5	0.1	0.31	6.4	0.1	0.30	6.2	0.1	0.30	5.3	0.1
0.33	7.8	0.0	0.34	7.0	0.0	0.34	6.4	0.0	0.34	6.1	0.1	0.33	5.8	0.1	0.34	4.9	0.1
0.38	7.6	0.0	0.39	6.7	0.0	0.39	6.4	0.0	0.39	6.1	0.1	0.39	5.4	0.1	0.39	5.0	0.1
0.43	7.3	0.0	0.44	6.9	0.0	0.44	6.0	0.0	0.44	5.8	0.1	0.44	5.4	0.1	0.44	3.9	0.1
0.48	7.2	0.0	0.49	7.1	0.0	0.49	6.3	0.0	0.49	6.3	0.1	0.49	5.3	0.1	0.54	3.9	0.1
0.53	7.3	0.0	0.54	6.8	0.0	0.55	6.3	0.1	0.54	5.8	0.1	0.54	5.4	0.1	0.59	3.5	0.1
0.58	7.2	0.0	0.59	7.0	0.0	0.60	6.2	0.1	0.59	5.9	0.1	0.59	5.4	0.1	0.64	3.9	0.1
0.63	7.2	0.0	0.64	6.9	0.0	0.65	6.3	0.1	0.65	6.0	0.1	0.64	5.3	0.1	0.69	4.6	0.1
0.69	7.2	0.0	0.69	7.2	0.0	0.70	6.3	0.1	0.70	6.2	0.1	0.69	5.9	0.1			

x/H = 0.63 $T_{inlet}=34.0°C$			x/H = 0.71 $T_{inlet}=33.7°C$			x/H = 0.79 $T_{inlet}=33.8°C$			x/H = 0.88 $T_{inlet}=34.0°C$			x/H = 0.96 $T_{inlet}=33.8°C$		
$\frac{y}{b}$	U	ΔT	$\frac{y}{b}$	U	ΔT	$\frac{y}{b}$	U	ΔT	$\frac{y}{b}$	U	ΔT	$\frac{y}{b}$	U	ΔT
0.00	0.0	3.1	0.00	0.0	3.4	0.00	0.0	3.4	0.00	0.0	3.0	0.00	0.0	2.8
0.01	7.2	2.0	0.03	11.8	1.6	0.02	9.0	2.1	0.03	8.0	1.7	0.05	11.0	1.2
0.03	13.6	1.1	0.05	15.5	1.0	0.03	13.9	1.2	0.05	11.3	1.3	0.07	13.7	1.0
0.05	15.6	0.7	0.06	16.0	0.7	0.05	15.6	0.8	0.06	14.3	0.9	0.09	14.6	0.8
0.06	15.4	0.5	0.08	15.4	0.5	0.07	15.6	0.7	0.08	15.2	0.7	0.10	14.4	0.7
0.08	14.8	0.4	0.10	14.5	0.4	0.09	14.9	0.5	0.10	15.1	0.6	0.12	14.1	0.6
0.10	13.3	0.3	0.11	13.9	0.4	0.10	14.0	0.5	0.11	14.8	0.5	0.14	12.8	0.6
0.12	12.5	0.3	0.13	12.8	0.3	0.12	13.3	0.4	0.13	13.7	0.5	0.17	11.4	0.5
0.13	11.4	0.2	0.15	11.9	0.3	0.14	11.9	0.4	0.15	13.1	0.4	0.20	10.8	0.5
0.15	10.4	0.2	0.18	10.1	0.3	0.17	10.4	0.3	0.18	11.5	0.4	0.24	9.3	0.4
0.18	8.9	0.2	0.21	9.1	0.3	0.20	9.1	0.3	0.22	10.2	0.3	0.27	8.4	0.4
0.22	7.5	0.1	0.25	7.5	0.2	0.24	7.6	0.3	0.25	8.8	0.3	0.31	7.2	0.4
0.25	6.7	0.1	0.28	6.8	0.3	0.27	6.4	0.3	0.28	7.7	0.3	0.36	6.1	0.4
0.28	6.1	0.1	0.31	5.5	0.5	0.31	5.2	0.4	0.32	7.0	0.3	0.41	5.4	0.4
0.32	5.0	0.1	0.36	3.8	0.4	0.36	4.1	0.4	0.37	5.8	0.3	0.46	4.7	0.3
0.37	3.8	0.1	0.41	3.4	0.4	0.41	3.0	0.4	0.42	4.8	0.3	0.51	4.7	0.3
0.42	3.4	0.1	0.46	2.4	0.5	0.46	2.6	0.4	0.47	4.3	0.3	0.56	5.2	0.3
0.47	3.3	0.1	0.51	2.6	0.3	0.51	2.5	0.3	0.52	4.3	0.2	0.61	5.8	0.3
0.52	3.2	0.1	0.56	2.7	0.1	0.56	2.7	0.3	0.57	4.6	0.3	0.66	6.6	0.4
0.57	3.7	0.1	0.61	3.5	0.1	0.61	3.7	0.3	0.62	5.3	0.3			
0.62	4.0	0.1	0.66	4.4	0.2	0.66	4.1	0.3	0.67	6.7	0.3			
0.67	4.9	0.1												

Table A.1: Mean velocity U (mm.s^{-1}) and temperature $\Delta T = T - T_{inlet}$ (°C) in the left half-channel, where T_{inlet} is the inlet temperature. $y/b = 0$ is the position of the left wall, $b = 59$ mm. Because measurements last almost one day for each level x/H, T_{inlet} exhibits small variations.

[1] C. Daverat, Y. Li, H. Pabiou, C. Ménézo, S. Xin, Transition to turbulent heat transfer in heated vertical channel - Scaling analysis, International Journal of Thermal Sciences, 112, (2017) 199–210.

[2] W. Elenbaas, Heat dissipation of parallel plates by free convection, Physica IX 39 (1) (1942) 1–28.

[3] J. R. Bodoia, J. F. Osterle, The delopment of free convection between heated vertical plates, Journal of Heat Transfer 84 (1962) 40–44.

[4] W. Aung, L. S. Fletcher, V. Sernas, Developing laminar free convection between vertical flat plates with asymmetric heating, Int. J. Heat Mass Transfer 15 (1972) 2293–2308.

[5] O. Miyatake, T. Fujii, M. Fujii, H. Tanaka, Natural convective heat transfer between vertical parallel plates - one plate with a uniform heat flux and the other thermally insulated, Heat Transfer Japaneese Research 1 (1973) 25–33.

[6] W. Aung, Fully developed laminar free convection between vertical plates heated asymmetrically, Int. J. Heat Mass Transfer 15 (1972) 1577–1580.

[7] B. Brinkworth, M. Sandberg, Design procedure for cooling ducts to minimise efficiency loss due to temperature rise in PV arrays, Solar Energy 80 (2006) 89–103.

[8] M. Miyamoto, Y. Katoh, J. Kurima, H. Sasaki, Turbulent free convection heat transfer from vertical parallel plates, in: Hemisphere (Ed.), International Heat Transfer Conference, Vol. 4, 1986, pp. 1593–1598.

[9] B. W. Webb, D. P. Hill, High Rayleigh number laminar natural convection in an asymmetrically heated vertical channel, Journal of Heat Transfer 111 (1989) 649–656.

[10] E. M. Sparrow, J. L. Gregg, Laminar free convection from a vertical plate with uniform surface heat flux, Transaction of the ASME 78 (1956) 435–440.

[11] M. A. Habib, S. A. M. Said, S. A. Ahmed, A. Asghar, Velocity characteristics of turbulent natural convection in symmetrically and asymmetrically heated vertical channels, Experimental Thermal and Fluid Science 26 (2002) 77–87.

[12] T. F. Ayinde, S. A. M. Said, M. A. Habib, Experimental investigation of turbulent natural convection flow in a channel, Heat Mass Transfer 42 (2006) 169–177.

[13] H. M. Badr, M. Habib, S. Anwar, R. Ben-Mansour, S. A. M. Said, Turbulent natural convection in vertical parallel-plate channels, Heat Mass Transfer 43 (2006) 73–84.

[14] M. Fossa, C. Ménézo, E. Leonardi, Experimental natural convection on vertical surfaces for building integrated photovoltaic (bipv) applications, Experimental Thermal and Fluid Science 32 (2008) 980–990.

[15] E. Sanvicente, S. Giroux, C. Ménézo, H. Bouia, Transitional natural convection flow and heat transfer in an open channel, International Journal of Thermal Sciences 63 (2013) 87–104.

[16] A. G. Fedorov, R. Viskanta, Turbulent natural convection heat transfer in an asymmetrically heated, vertical parallel-plate channel, Int. J. Heat Mass Transfer 40 (1997) 3849–3860.

[17] X. Cheng, U. Müller, Turbulent natural convection coupled with thermal radiation in large vertical channels with asymmetric heating, Int. J. Heat Mass Transfer 41 (1998) 1681–1692.

[18] T. Yilmaz, S. M. Fraser, Turbulent natural convection in a vertical parallel-plate channel with asymmetric heating, Int. J. Heat Mass Transfer 50 (2007) 2612–2623.

[19] G. Desrayaud, E. Chénier, A. Joulin, A. Bastide, B. Brangeon, J. Caltagirone, Y. Cherif, R. Eymard, C. Garnier, S. Giroux-Julien, Y. Harnane, P. Joubert, N. Laaroussi, S. Lassue, P. Le Quéré, R. Li, D. Saury, A. Sergent, S. Xin, A. Zoubir, Benchmark solutions for natural convection flows in vertical channels submitted to different open boundary conditions, International Journal of Thermal Sciences 72 (2013) 18–33.

[20] R. A. Wirtz, R. J. Stutzman, Experiments on free convection between vertical plates with symmetric heating, Journal of Heat Transfer 104 (1982) 501–507.

[21] A. Bar-Cohen, W. M. Rohsenow, Thermally optimum spacing of vertical, natural convection cooled, parallel plates, Journal of Heat Transfer 106 (1984) 116–123.

[22] C. Daverat, H. Pabiou, C. Ménézo, H. Bouia, S. Xin, Experimental investigation of turbulent natural convection in a vertical water channel with symmetric heating: Flow and heat transfer, Experimental Thermal and Fluid Science 44 (2013) 182–193. doi:10.1016/j.expthermflusci.2012.05.018.

[23] X.-D. Shang, X.-L. Qiu, P. Tong, K.-Q. Xia, Measured local heat transport in turbulent Rayleigh-Bénard convection, Physical Review Letters 90 (2003) 074501. doi:10.1103/PhysRevLett.90.074501.

[24] X.-D. Shang, P. Tong, K.-Q. Xia, Scaling of the local convective heat flux in turbulent Rayleigh-Bénard convection, Physical Review Letters 100 (2008) 244503. doi:10.1103/PhysRevLett.100.244503.